

Broadband 3D optical modeling of HgCdTe infrared focal plane arrays

Marco Vallone¹, Andrea Palmieri¹, Marco Calciati¹, Francesco Bertazzi^{1,2}, Federica Cappelluti¹, Giovanni Ghione¹, Michele Goano^{1,2}, Stefan Hanna³, Heinrich Figgemeier³, Robert Scarmozzino⁴, Evan Heller⁴ and Mayank Bahl⁴

¹ Dipartimento di Elettronica e Telecomunicazioni, Politecnico di Torino, corso Duca degli Abruzzi 24, 10129 Torino, Italy

² IEIIT-CNR, Politecnico di Torino, corso Duca degli Abruzzi 24, 10129 Torino, Italy

³ AIM Infrarot-Module GmbH, Theresienstraße 2, 74072 Heilbronn, Germany

⁴ Synopsys, Inc., 400 Executive Blvd, Ossining, NY, USA

Email: marco.vallone@polito.it, mayank.bahl@synopsys.com, stefan.hanna@aim-ir.com

Abstract- We present a modeling technique for the efficient broadband simulation of infrared HgCdTe-based focal plane arrays. The approach performs a single broadband FullWAVE™ FDTD optical simulation and a series of discrete Fourier transforms for obtaining absorbed photon density profiles on a set of frequencies. These distributions are then aggregated, through a weighted average, and imported as a generation term into a single Sentaurus Device electrical simulation, which calculates the corresponding photocurrent and inter-pixel crosstalk. This technique can save an order of magnitude in memory and computation time compared to performing multiple monochromatic optical and electrical simulations.

I. INTRODUCTION

The current development of infrared (IR) HgCdTe-based focal plane arrays (FPAs) with sub-wavelength pixel pitch [1–4] aims at FPAs with pixel size $d = 5\text{--}6 \mu\text{m}$ for long-wavelength IR detectors (LWIR, cutoff wavelength $\lambda_c = 8\text{--}14 \mu\text{m}$) and $d = 2\text{--}3 \mu\text{m}$ for mid-wavelength ones (MWIR, $\lambda_c = 3\text{--}5 \mu\text{m}$). We have recently investigated [5] with 3D numerical simulations the spectrally-resolved optical response and inter-pixel crosstalk of a 5×5 LWIR $n\text{-on-}p$ $\text{Hg}_{0.774}\text{Cd}_{0.226}\text{Te}$ array with $d = 5 \mu\text{m}$ under *monochromatic* illumination, using both plane waves and focused sources. In the present work, the optical response of the same array is determined under *nonmonochromatic* focused illumination. As in [5–7], the Sentaurus Device numerical simulator by Synopsys [8] is employed to solve the electrical problem within the drift-diffusion (DD) framework, taking into account the composition, doping, and temperature dependence of the HgCdTe alloy at 77 K. The optical generation rate G_{opt} due to the illumination enters as a source term in the DD continuity equations, and is taken equal to the absorbed photon density A_{opt} . Here A_{opt} is evaluated by the finite difference time domain (FDTD) algorithm as implemented in FullWAVE™ [9], a commercially available optical software tool with seamless integration to the Sentaurus Device workflow. The response to nonmonochromatic illumination sources may be addressed in two ways, which are described in Sec. II and III below.

II. AGGREGATED MONOCHROMATIC SIMULATIONS

The most general and direct approach is to make multiple single-frequency optical and electrical simulations over the desired frequency range. The 5×5 LWIR array was illuminated with a normally incident Gaussian beam with a beam waist w_0

of $3.4 \mu\text{m}$. A total of $N=65$ monochromatic optical and electrical simulations were performed over the frequency range $v = 30\text{--}150 \text{ THz}$ ($\lambda \cong 2\text{--}10 \mu\text{m}$). In the FullWAVE™ FDTD simulations, convolutional perfectly matched layer (CPML) boundary conditions were used in all directions. At each frequency v_i , we obtained an absorbed photon density rate $A_{\text{opt}}(v_i)$ through optical simulation, assuming the same power being launched at each frequency. The absorbed photon density profiles at three of these frequencies ($v_i \cong 120, 75, 45 \text{ THz}$, corresponding to $\lambda_i \cong 2.5, 4, 6.667 \mu\text{m}$) are shown in Fig. 2(a), (b), and (c), respectively.

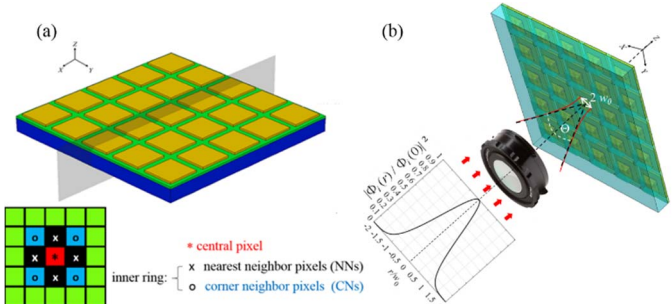


Fig. 1 (a) The simulated 5×5 HgCdTe array, and (b) the illuminating Gaussian beam focused on the central pixel of the array.

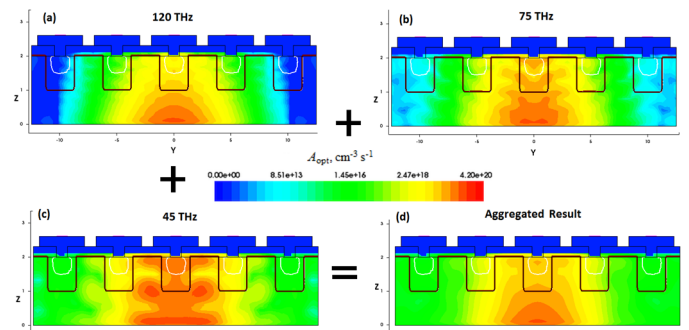


Fig. 2. Panels (a,b,c), A_{opt} distributions obtained by FullWAVE™ at $v \cong 120, 75$ and 45 THz ($\lambda \cong 2.5, 4, 6.667 \mu\text{m}$), respectively. In panel (d), the aggregated $A_{\text{opt},\text{agg}}$ resulting from the sum of 65 rates in the interval $v \cong 30\text{--}150 \text{ THz}$ ($\lambda \cong 2\text{--}10 \mu\text{m}$).

At each frequency in the range of interest, the associated A_{opt} was imported into Sentaurus Device, which was used to solve the carrier transport equations. The photocurrent I_{ph} collected by the central pixel (CP), its nearest neighbors (NNs), and the

corner neighbors (CNs) is shown in Fig. 3 (red stars, black crosses and blue circles, respectively). This allows for the investigation of the inter-pixel electrical and optical crosstalk, whose expressions can be found in [5], Eqs. (19, 20).

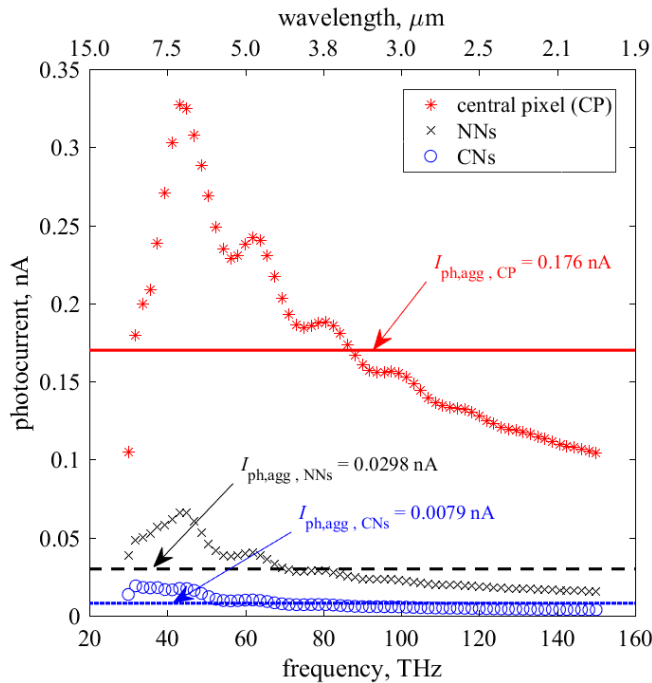


Fig. 3. The simulated photocurrent spectra $I_{\text{ph}}(v_i)$ obtained using the $A_{\text{opt}}(v_i)$. Red stars refer to the central pixel, black crosses and blue circles to nearest and corner neighbors, respectively. The corresponding $I_{\text{ph,agg}}$ obtained from $A_{\text{opt,agg}}$ are shown as horizontal lines (red solid line for CP, black dashed line for NNs, blue dotted line for CNs).

The effect of a nonmonochromatic (broadband) optical source may be obtained by summing the rates $A_{\text{opt}}(v_i)$ according to $A_{\text{opt,agg}} = \frac{1}{N} \sum_{i=1}^N A_{\text{opt}}(v_i)$. Fig. 2(d) reports the $A_{\text{opt,agg}}$ distribution, which includes the contributions of all 65 monochromatic optical simulations. In Fig. 3, the photocurrent $I_{\text{ph,agg}}$, obtained from DD simulations using $A_{\text{opt,agg}}$, is shown for each type of pixel (horizontal lines): $I_{\text{ph,agg}} \cong 0.176 \text{ nA}$ for CP, $I_{\text{ph,agg}} \cong 0.0298 \text{ nA}$ for NNs, $I_{\text{ph,agg}} \cong 0.0079 \text{ nA}$ for CNs. We note that, since the optical flux is quite low, despite the nonlinearity of the electrical problem treated in the DD framework, the $I_{\text{ph,agg}}$ obtained for each pixel is very close to the weighted average $\frac{1}{N} \sum_{i=1}^N I_{\text{ph}}(v_i)$.

III. BROADBAND SIMULATIONS

In order to save on computational resources (CPU time and memory), we considered also the alternative approach to obtain the aggregate result through a single optical and electronic simulation. This approach uses, for the optical input, a very narrow time-domain Gaussian pulse $\varphi(x, y; t)$ and a series of discrete Fourier transforms (DFTs) to obtain the response at each frequency. In this way, a single broadband FullWAVE™ FDTD simulation can produce the N distributions $A_{\text{opt}}(v_i)$ in a user-defined frequency interval. These can be aggregated in a

way identical to the one described in Sec. II for the monochromatic simulations. The $A_{\text{opt,agg}}$ thus obtained is used as input for a single drift-diffusion device simulation, yielding $I_{\text{ph,agg}}$. This approach can save an order of magnitude in simulation time depending on the number of simulated frequencies. The $A_{\text{opt,agg}}$ calculated through this approach with a single broadband simulation [9] is shown in Fig. 4.

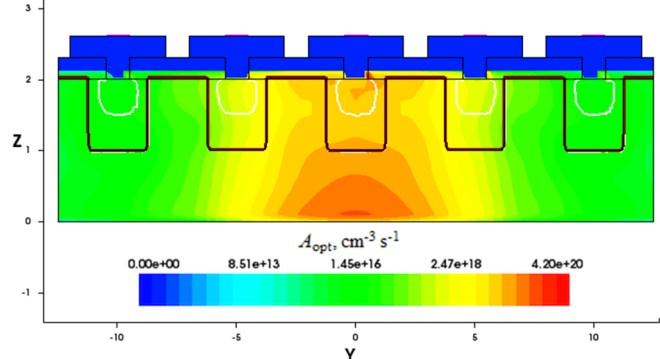


Fig. 4. $A_{\text{opt,agg}}$ resulting from the sum of 65 rates obtained via DFT in the interval $v = 30–150 \text{ THz}$ ($\lambda \cong 2–10 \mu\text{m}$) with a single broadband FDTD calculation.

The result agrees well with the $A_{\text{opt,agg}}$ obtained from the monochromatic scan from Fig. 2(d). Regarding the electrical results, we obtained $I_{\text{ph,agg}} \cong 0.174, 0.0301, 0.0082 \text{ nA}$ for CP, NNs and CNs, respectively, in excellent agreement with the aggregated results from the monochromatic approach shown in Fig. 3 by horizontal lines. It should be noticed that this broadband approach still produces all the optical spectral information contained in the $A_{\text{opt}}(v_i)$ rates, and just one electrical simulation is needed to obtain other quantities such as the aggregated photocurrent $I_{\text{ph,agg}}$ or the corresponding quantum efficiency.

REFERENCES

- [1] R. G. Driggers, R. Vollmerhausen, J. P. Reynolds, J. Fanning, G. C. Holst, “Infrared detector size: how low should you go?”, *Opt. Eng.*, vol. 51, p. 063202, 2012.
- [2] G. C. Holst, R. G. Driggers, “Small detectors in infrared system design,” *Opt. Eng.*, vol. 51, p. 096401, 2012.
- [3] W. E. Tenant, D. J. Gulbransen, A. Roll, M. Carmody, D. Edwall, A. Julius, P. Drieske, A. Chen, W. McLevige, S. Freeman, D. Lee, D. E. Cooper, E. Piquette, “Small-pitch HgCdTe photodetectors,” *J. Electron. Mater.*, vol. 43, pp. 3041–3046, 2014.
- [4] A. Rogalski, P. Martyniuk, M. Kopytko, “Challenges of small-pixel infrared detectors: a review,” *Rep. Prog. Phys.*, vol. 79, p. 046501, 2016.
- [5] M. Vallone, M. Goano, F. Bertazzi, G. Ghione, W. Schirmacher, S. Hanna, H. Figgemeier, “Simulation of small-pitch HgCdTe photodetectors,” *J. Electron. Mater.*, vol. 46, 2017, doi:10.1007/s11664-017-5378-z.
- [6] M. Vallone, M. Mandurrino, M. Goano, F. Bertazzi, G. Ghione, W. Schirmacher, S. Hanna, H. Figgemeier, “Numerical modeling of SRH and tunneling mechanisms in high-operating-temperature MWIR HgCdTe photodetectors,” *J. Electron. Mater.*, vol. 44, p. 3056, 2015.
- [7] M. Vallone, M. Goano, F. Bertazzi, G. Ghione, W. Schirmacher, S. Hanna, H. Figgemeier, “Comparing FDTD and ray tracing models in the numerical simulation of HgCdTe LWIR photodetectors,” *J. Electron. Mater.*, vol. 45, p. 4524, 2016.
- [8] Synopsys Sentaurus™ Process and Device simulation platform.
- [9] FullWAVE™ User Guide, Synopsys, Inc, RSoft Products. (2017).